Comparative analysis of delamination resistance in CFRP laminates interleaved by thermoplastic nanoparticle

Evaluating toughening mechanisms in modes I and II

Mohammadi, Reza; Akrami, R.; Assaad, Maher; Imran, Ahmed; Fotouhi, Mohammad

DOI
10.1016/j.jcomc.2024.100518

Publication date
2024

Document Version
Final published version

Published in
Composites Part C: Open Access

Citation (APA)
Mohammadi, R., Akrami, R., Assaad, M., Imran, A., & Fotouhi, M. (2024). Comparative analysis of delamination resistance in CFRP laminates interleaved by thermoplastic nanoparticle: Evaluating toughening mechanisms in modes I and II. *Composites Part C: Open Access*, *15*, Article 100518. https://doi.org/10.1016/j.jcomc.2024.100518

Composites Part C: Open Access 15 (2024) 100518

Contents lists available at ScienceDirect

Composites Part C: Open Access

journal homepage: www.sciencedirect.com/journal/composites-part-c-open-access

Comparative analysis of delamination resistance in CFRP laminates interleaved by thermoplastic nanoparticle: Evaluating toughening mechanisms in modes I and II

Reza Mohammadi [a,*], R Akrami [b], Maher Assaad [c], Ahmed Imran [d], Mohammad Fotouhi [a]

[a] Faculty of Civil Engineering and Geosciences, Delft University of Technology, 2628, CD, Delft, Netherlands
[b] Department of Mechanical and Aerospace Engineering, University of Strathclyde, 75 Montrose Street, Glasgow, G1 1XJ, UK
[c] Department of Electrical and Computer Engineering, College of Engineering and IT, Ajman University, Ajman, P.O. Box 346, United Arab Emirates
[d] Department of Biomedical Engineering, College of Engineering and IT, Ajman University, Ajman, P.O. Box 346, United Arab Emirates

ARTICLE INFO

Keywords:
CFRP laminates
Fracture toughness
Thermoplastic nanoparticles
Polysulfone nanofiber

ABSTRACT

The study considers the delamination resistance of carbon/epoxy laminates modified with Thermoplastic Nanoparticles of Polysulfone (TNPs). A new electrospinning nanofiber technique was utilized to convert polysulfone polymer into nanoparticles and uniformly disperse them within the resin. Fracture toughness was evaluated under loading modes I and II. In mode I, the toughness (G_{IC}) increased significantly from 170 to 328 J/m^2 with TNPs incorporation. However, mode II showed minimal change, with G_{IIC} values of 955 J/m^2 for virgin and 950 J/m^2 for TNPs-modified specimens. Scanning Electron Microscopy (SEM) was employed to depict the influence of TNPs on damage characteristics and crack propagation patterns. In mode I, crack deviation enhanced toughness as TNPs bypassed the PSU, while in mode II, cracks propagated through TNPs, resulting in particle smearing on the epoxy surface. This highlights TNPs' potential to modify the fracture toughness in mode I loading, but their effect is constrained in mode II loading scenarios.

1. Introduction

Interlaminar cracks (Delamination) are the significant forms of damage features in the composite structures [1-3]. Delamination of composite structures often arises from various factors like with such as impact loading [4-6], fatigue loading [7-10], thermal effects [11-13], free edge interlaminar stress [14-17], tapered structures [18-20] and manufacturing effects like drilling [21-23]. Typically, delamination behavior is assessed through the examination of resistance to inter-laminar crack growth and fracture toughness. The fracture toughness is defined as the rate of strain energy released during crack propagation [24,25]. Higher fracture toughness values denote enhanced resistance to crack propagation within the composite. Various fracture tests, including mode I [26], mode II [27], Mixed mode I & II [28], and mode III [29], are commonly employed to examine the resistance to delamination in composite laminates. Additionally, the pull-off test [30] finds utility in industry and applied structures to evaluate the adhesive strength between laminates.

Over the past few years, numerous researchers have concentrated on enhancing delamination resistance and improving fracture toughness in composite materials. Strategies employed by researchers include the utilization of Z-pins [31,32], 3D woven composite [33,34], stitching [35-37], nanofibers [38-41], and nanoparticles. Various nanoparticles, including CNT [42], Al_2O_3 [43] and TiO_2 [44] have been employed by researchers to enhance fracture toughness of composite laminates. For instance, Liu et al. [45] illustrated the improvement in the fracture toughness of CFRP materials by adding CNT and graphene oxide nanoparticles. Their findings indicate that the addition of MWCNTs/GO nanoparticles resulted in an increase in G_{IC} by up to 151 % and G_{IIC} by up to 156 %. Furthermore, Prasad et al. [46] employed titanium dioxide (TiO_2) nanoparticles into flax fiber composite laminates, leading to a respective increase in fracture toughness by 52 % and 73 % under mode I and mode II conditions. The SEM images illustrated that the dispersion of nanoparticles within the fiber matrix interface establishes a mechanical interlock, thereby enhancing the adhesion of fiber/matrix bonding. Consequently, this leads to an enhanced fracture toughness in both mode I and mode II. The main novelty of this research work is to consider the effect of thermoplastic nanoparticle on the mode I and

* Corresponding author at: TUDelft, Delft, Netherlands.
E-mail address: rezam75@gmail.com (R. Mohammadi).

https://doi.org/10.1016/j.jcomc.2024.100518

Available online 26 September 2024

mode II fracture toughness of composite laminates.

Most nanoparticles utilized in composite materials are ceramic-based and possess high hardness, dispersed within the resin via ultrasonic methods. However, the utilization of polymer-based nanoparticles to enhance delamination resistance has received much less attention from researchers. The reasons for this are the limitations in producing thermoplastic nanoparticles and the challenge of achieving a uniform distribution of polymeric nanoparticles throughout the resin. The primary innovation of this research is the use of thermoplastic nanoparticles to assess the mode I and mode II fracture toughness of composite laminates. Consequently, this study focuses on employing Thermoplastic Nanoparticles of Polysulfone (TNPs) in carbon/epoxy laminates to consider the fracture toughness and evaluate toughening mechanisms. An innovative method was used to produce nanoparticles from polysulfone pellets as a thermoplastic material, and to uniformly distribute them within the thermoset resin. To this aim, polysulfone pellets were first converted into nanofibers and then the nanofibers were placed between the composite layers.

Throughout the curing process, the resin permeated the pores of the nanofibers. Subsequently, as the temperature increased, the polysulfone nanofiber melted, enabling it to be uniformly and homogeneously distributed as nanoparticles within the brittle epoxy resin.

Subsequently, both mode I and mode II tests were conducted to determine the interlaminar fracture toughness. Results showed 1.9 times enhancement in mode I fracture toughness values (G_{IC}), while surprisingly, there was no significant change observed in mode II fracture toughness (G_{IIC}) values. The SEM micrographs indicated that during mode I loading, the crack path continuously altered the crack continuously changes its direction due to contact with polysulfone Nanoparticle, thus increasing the delamination resistance. Conversely, in mode II condition, the crack propagated directly and passed through polysulfone sphere particles. In this instance, the thermoplastic nanoparticles exhibited weakened resistance due to shear loading, resulting in their smearing on the fracture surface. Finally, this research demonstrates that thermoplastic nanoparticles can improve mode I fracture toughness without altering mode II toughness in composite laminates.

2. Preparation of specimens

The unidirectional carbon/epoxy Prepreg (AS4/8552), was utilized to produce composite samples. This type of Prepreg is a high-performance material suitable for applications in aerospace industry. The epoxy system employed within this Prepreg, HexPly® 8552, undergoes complete curing at 180 °Celsius. The tensile elastic modulus for this type of prepreg is 141 GPa in the 0° direction and 10 GPa in the 90° direction [47]. Manual layup was employed, utilizing 24 layers in total. To facilitate DCB (mode I) and ENF (mode II) tests in accordance with ASTM standards, an initial pre-crack was introduced. This pre-crack was generated by incorporating a 13-micron thick Teflon layer in the middle of laminate. Additionally, in modified specimens, a 60-micron thick polysulfone nanofiber sheet was positioned along the continuation of the initial pre-crack. To ensure consistency and minimize manufacturing errors, all samples were fabricated simultaneously. Subsequently, the laminates were thoroughly vacuumed and placed in an autoclave for the curing cycle. Following this process, the manufactured sheets were cut to standard dimensions of 180×25 mm^2. The thickness of the samples was determined to be 4.5 mm, as measured by a caliper. In order to uniformly distribute soft polysulfone as a thermoplastic material inside the brittle epoxy as a thermosetting material, first polysulfone was produced in the form of nanofibers. For this purpose, the electrospinning technique was utilized. Further information regarding the preparation of the solution, choice of solvent, and electrospinning parameters can be found in [48].

Nanofibers have a porous structure and the resin has the ability to penetrate into the cavities. While curing the composite laminate at 180°, the nanofibers are melted inside the matrix and distributed as nanoparticles in the brittle matrix. In the Fig. 1, the mechanism of dispersion and distribution of nanoparticles into the matrix is shown. Fig. 1-A shows the curing process of Hexply@8552 Prepreg material according to manufacturer datasheet [47]. As seen the curing process divided to 5 steps based on temperature graph changes. Initially, the temperature is raised gradually at a rate of 1 °C/min from the 25 (room temperature) up to 110 °Celsius, where it is maintained for one hour. Subsequently, the temperature is increased steadily at a rate of 1° per minute until reaching 180 °Celsius, and it is held at this level for two hours.

As depicted in Fig. 1-B, illustrating the relationship between temperature and viscosity changes, the epoxy resin's viscosity decreases with rising temperature, facilitating its penetration into the porous structure of nanofibers, as shown in Fig. 1-C. During steps 2 and 3, lasting nearly two hours, the resin exhibits minimal viscosity, enabling it to permeate all the nanofiber porous and achieve complete wetting. Moreover, the elevation of the temperature to 180 °Celsius and its maintenance at this level induces the melting of polysulfone nanofibers. The surface tension of polysulfone causes the molten particles to adopt a spherical shape, distributing uniformly within the epoxy matrix, as illustrated in Fig. 1-D.

3. Methodology of fracture test

This section presents the methodology for conducting mode I and mode II tests, which established by ASTM standard. Mode I tests, were performed by ASTM D5528–13 [49] guidelines. In accordance with this standard, the tests were carried out in the form of displacement-control at 1 mm per minute. During tests, the values of displacements and loads were recorded, and crack growth was also documented by a camera. Aluminum and steel parts were employed at the ends of the arms to apply the load, as depicted in Fig. 2-A. Mode II fracture tests were also carried out following ASTM D7905 [50] guidelines. These tests utilized End Notched Flexure (ENF) specimens and were carried out using a 3-point bending test setup (Fig. 2-B). To ensure stable crack growth during mode II tests, a lower displacement rate of 0.5 mm/min was chosen. All testing procedures were conducted in the DASML laboratory at Delft University of Technology, utilizing a 10 kN hydraulic test machine (MTS 810 model).

4. Mode I test results

Fig. 3 shows the load-displacement graphs for all mode I tests. Notably, it's observed that in the linear area the slope of curves is same for all specimens, suggesting that the presence of nanoparticles has no impact on slope, indicating an equivalent effective modulus across all specimens. Upon reaching the maximum or critical load (P_{cr}), crack initiation occurs, followed by a subsequent decrease in load. The critical load values averaged 75 N for reference samples and 101 N for TNPs-interleaved samples, representing a noteworthy 1.34-fold enhancement. Notably, reference specimens experienced a sudden load drop after the maximum load, attributed to an enrichment of resin at the initial crack tip, suggesting rapid crack length growth. Conversely, this sudden load drop was mitigated in TNPs-modified samples due to the inclusion of thermoplastic nanoparticles. In other words, in this type of sample, as the load gradually decreases, the compliance parameter, defined as displacement divided by load ($C=\delta/P$), gradually increases. In the elastic region, compliance remains constant, but when a crack begins to propagate, the load decreases, leading to an increase in compliance (see table 1). In reference specimens, a sudden load drop causes a sharp rise in compliance values, which is less favorable for a structure. A gradual increase in compliance near the fracture point is beneficial for materials, as it aids in diagnosing failure time and helps prevent catastrophic structural failure.

To calculate the fracture toughness (G_{IC}), the instruction recommended by ASTM D5528 was employed. Eq. (1) illustrates the

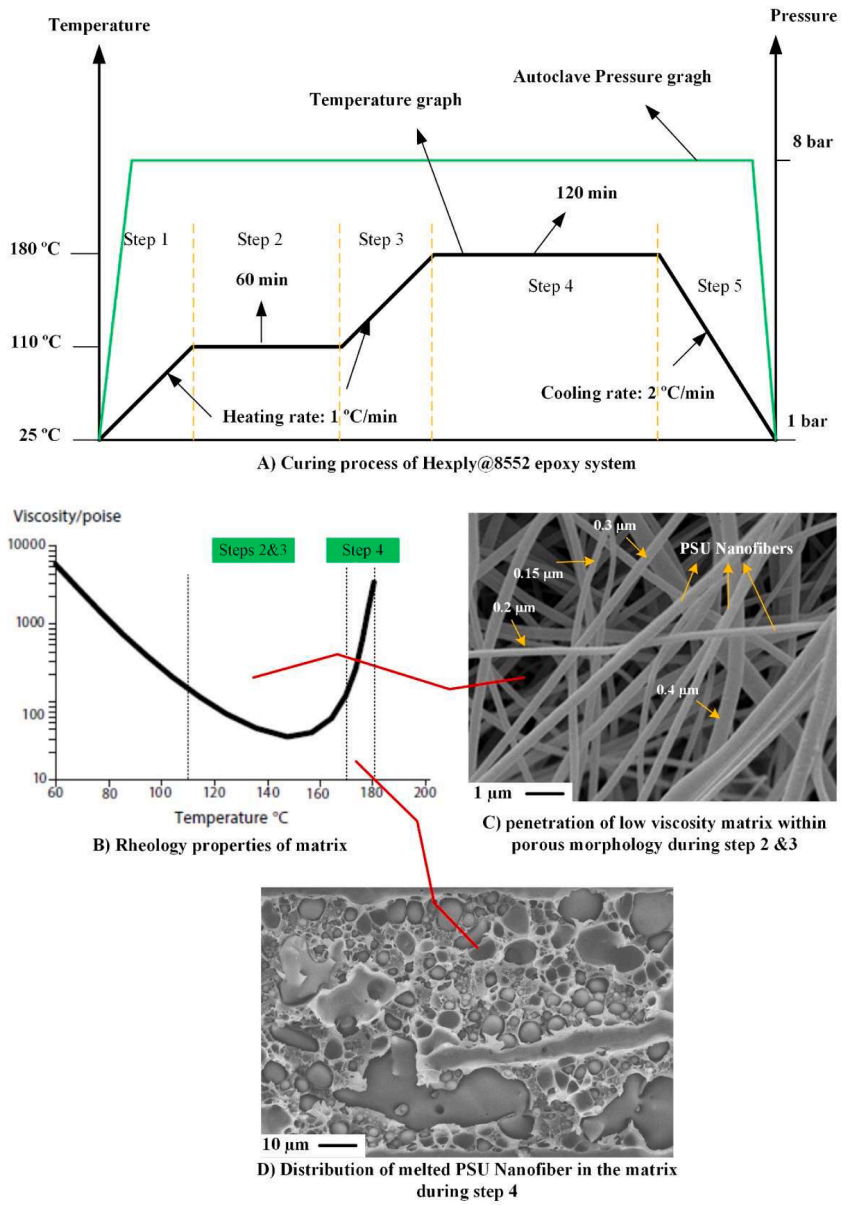

Fig. 1. Penetration mechanism of epoxy resin within porous PSU nanofiber mat and its melting into nanoparticles distributed in the resin.

calculation of G_{IC}. In this equation, P_{cr} shows the maximum load, δ_{cr} indicates the value of displacement at maximum load, B denotes the test sample width, a_0 signifies the pre-crack length, and Δ represents the crack length correction parameter, all of which are further detailed in ASTM D5528 [49].

$$G_{IC} = \frac{3P_{cr}\delta_{cr}}{2B(a_0 + \Delta)} \quad (1)$$

To calculate the Δ values, specific points have been chosen from the segment of crack propagation in the load-displacement curves. At these points, the crack growth (Δa) was initially identified using images captured by a digital camera (See Fig. 4). Subsequently, the crack length (a) was calculated as $a_0 + \Delta a$. Additionally, the corresponding values of displacements (δ) and loads (P), recorded by the testing machine, were extracted. The compliance was then calculated by dividing displacement by load ($C=\delta/P$) for all selected points. Next, the cube root of compliance ($C^{1/3}$) was computed. Table 1 presents the calculated values of important factors for PSU-1 sample (as an example), including crack growth, crack length, displacement, force, and compliance at each recorded moment.

Finally, the third root of compliance ($C^{1/3}$) is graphed against the delamination crack length. Fig. 5 depicts the linear correlation between these factors, accompanied by the Δ values for the TNPs-modified sample (PSU-1).

Table 2 presents key factors and also calculated G_{IC} values for all mode I test samples. The data indicate an average fracture toughness of 170 J/m^2 for virgin samples and 328 J/m^2 for TNPs-modified samples. This represents a significant 1.9-fold improvement in fracture toughness resulting from the inclusion of thermoplastic nanoparticles.

5. The result mode II tests

Fig. 6 illustrates the load-displacement diagram related to mode II tests conducted on both the reference and the nanoparticles TNPs-interleaved samples. As depicted in this figure, unlike mode I loading, mode II loading exhibits a sharp and sudden decrease in load curve after reaching the maximum point, indicative of rapid crack growth and propagation in this loading condition. Additionally, force values at the fracture moment are notably higher than those observed in mode I.

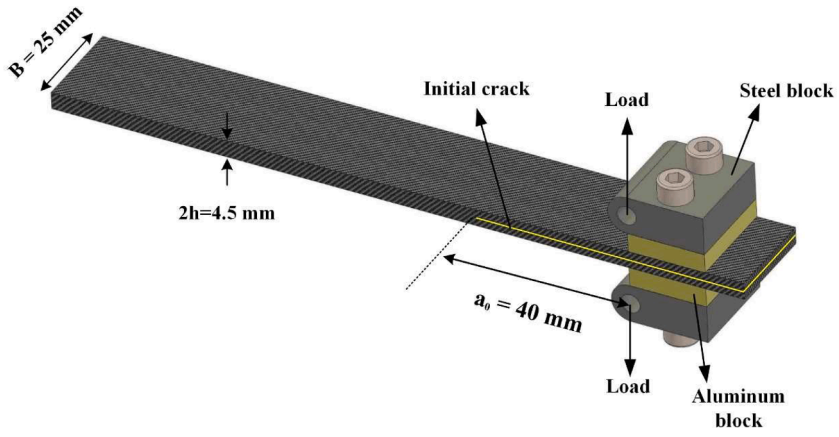

(A)

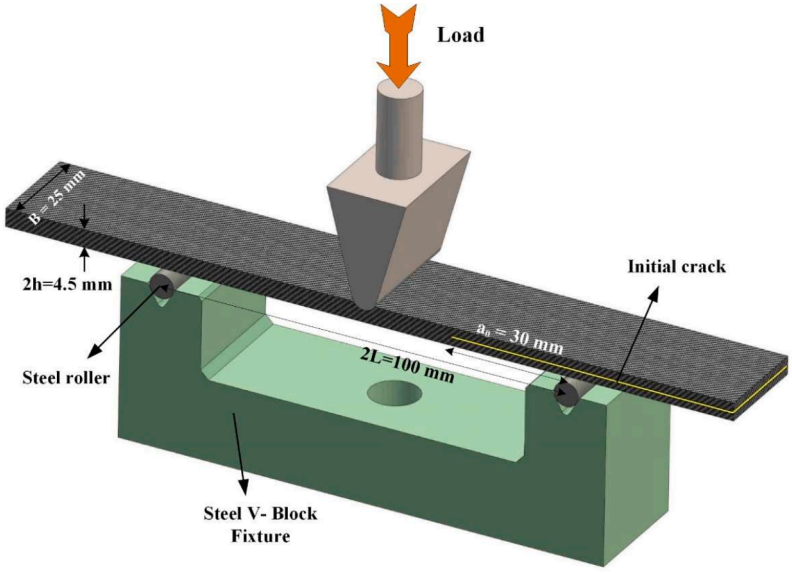

(B)

Fig. 2. Schematically test setup for Mode I (A) and Mode II (B) loading.

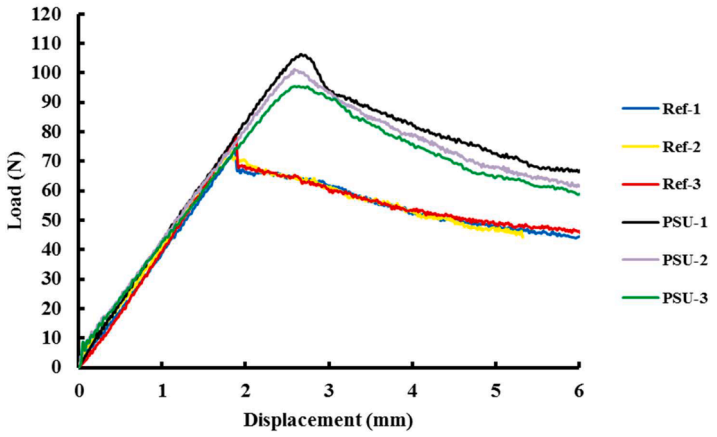

Fig. 3. The load-displacement graphs of all mode I test specimens.

Table 1
Calculateing of mode I fracture test parameters at different selected point versus time (PSU-1 sample).

Time (S)	Δa (mm)	a (mm)	Displacement (mm)	Load (N)	Compliance (mm/N)	$C^{1/3}$ $(mm/N)^{1/3}$	G_R (J/m^2)
0	0	40	0	0	–	–	–
160	1	41	2.66	106.37	0.0250	0.2924	361
200	5	45	3.33	87.09	0.0382	0.3369	334
250	11	51	4.16	79.21	0.0525	0.3746	341
300	17	57	5.00	69.95	0.0714	0.4150	327
350	21	61	5.83	67.17	0.0868	0.4428	345
400	27	67	6.66	61.15	0.1090	0.4777	330
450	31	71	7.50	57.90	0.1295	0.5059	333

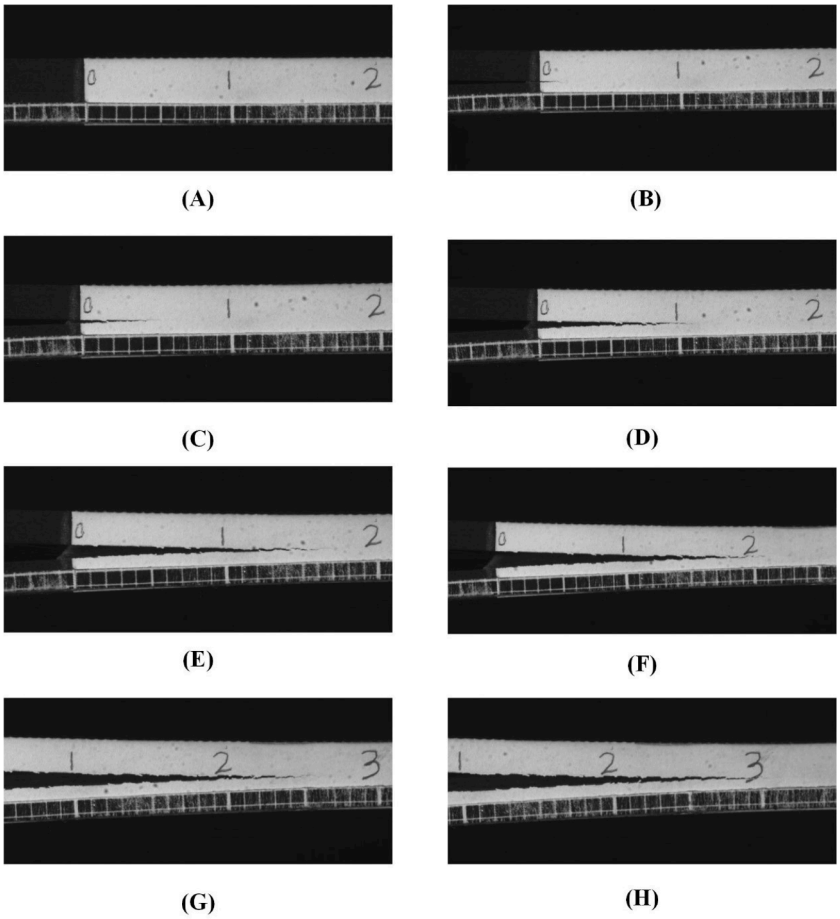

Fig. 4. The crack length propagation during the mode I test for PSU-1 specimen over time: A) $t = 0$ s, B) $t = 160$ s (crack starts to propagate), C) $t = 200$ s, D) $t = 250$ s, E) $t = 300$ s, F) $t = 350$ s, G) $t = 400$ s, H) $t = 450$ s.

surprisingly, the force and displacement values at the fracture moment for both the reference and TNPs modified samples show minimal variation. In fact, in mode II, unlike mode I, the presence of polysulfone nanoparticles does not contribute to an increase in maximum fracture load. The average maximum load values are 1096 N for virgin samples and 1100 for TNPs samples, with corresponding average displacement values of 2.05 mm and 2.07 mm, respectively, indicating minimal variation between the two. However, a notable observation is the presence of non-linearity in the load-displacement graph before the significant drop in load, leading to increased compliance in the Nano-modified samples. This increase in compliance is beneficial in preventing catastrophic failure in composite structures. Additionally, the slopes of curves for both reference and modified samples are almost same, suggesting that Polysulfone nanoparticles have negligible effect on the effective stiffness.

In order to determine the mode II fracture toughness (G_{IIC}), it is done according to the recommended instructions outlined in ASTM D7905 [50] standard. This standard provides the following relationship (Eq. (2)). Where P_{cr} is the maximum force, a_0 is the initial crack length, m is the compliance calibration (CC) parameter obtained in the subsequent section and B is the specimen width.

$$G_{IIC} = \frac{3mp_{cr}^2 a_0^2}{2B} \tag{2}$$

As observed, the parameter "m" is required to calculate the mode II fracture toughness using Eq. (2). This parameter is established through compliance tests conducted on samples as per standard procedures. Initially, samples are subjected to loading by crack length of 20 mm until reaching a force of 500 N, followed by unloading without any failure or crack growth within specimen. This process is replicated for crack lengths of 30 mm and 40 mm. Subsequently, force-displacement diagrams are plotted for these three states. The non-linear sections of the graphs are eliminated, and the slope of the linear segment is calculated

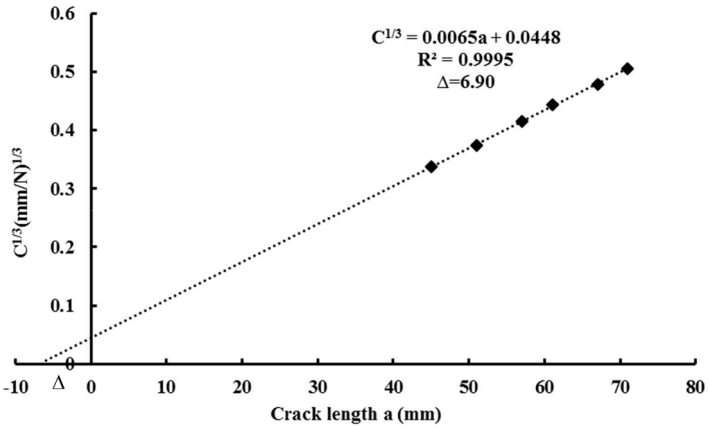

Fig. 5. Calculation of crack length correction parameter (Δ) using the third root of compliance for TNPs modified Specimen (PSU-1).

Table 2
Fracture toughness results of test specimens in mode I loading condition.

Sample	P_{cr} (N)	δ_{cr} (mm)	B (mm)	a_0 (mm)	Δ (mm)	G_{IC} (J/m^2)	Ave. P_{cr} (N)	Ave. G_{IC} (J/m^2)
Ref-1	74.26	1.85	25	40	8.43	170	75.64±2.39	169.6 ± 8.5
Ref-2	73.67	1.81	25	40	10.25	159	CV=0.03	CV=0.05
Ref-3	79.01	1.88	25	40	9.36	180		
PSU-1	106.37	2.66	25	40	6.90	361	101.04±4.45	328.6 ± 23.3
PSU-2	101.27	2.58	25	40	9.16	318	CV=0.04	CV=0.07
PSU-3	95.48	2.61	25	40	8.67	307		

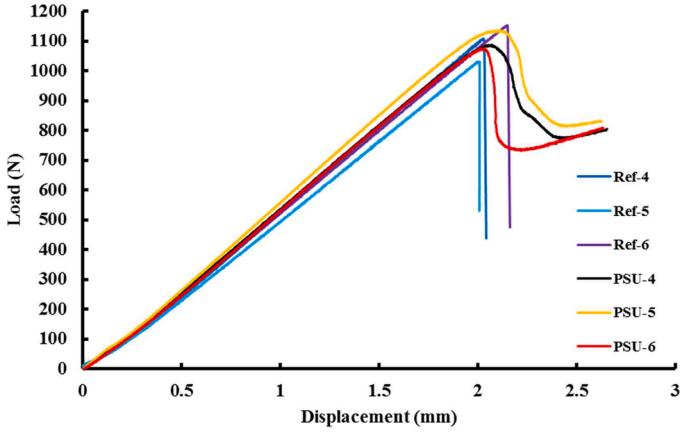

Fig. 6. The Mode II load-displacement graphs for all virgin and TPNs-modified samples.

by passing a line across the points (see Fig. 7-A). The inverse of this slope actually shows the amount of compliance for each initial crack length. Additionally, compliance is graphed against the third power of the initial crack length, and then a line was fitted through these points, as illustrated in Eq. (3), which A and m denote the parameters from the compliance tests.

$$C = A + ma^3 \tag{3}$$

Fig. 7-B shows the fitted line and the value of m for PSU-4 modified specimen. The specifics regarding compliance measurement and the determination of constants in the compliance equation are outlined in [50].

Table 3 displays the average G_{IIC} values across all specimens, indicating an average fracture toughness of 955 J/m^2 for reference samples and 950 J/m^2 for TNPs-modified samples. These results demonstrate minimal deviation in fracture toughness values, suggesting that thermoplastic nanoparticles don't significantly affect mode II fracture toughness, unlike mode I.

6. Results of fractography method

The micrographs captured by SEM were utilized to analyze the fractured surfaces and associated damage mechanisms in both reference samples and samples modified with TNPs. Subsequently, the damage characteristics of mode I and mode II were compared. Fig. 8 illustrates the fracture surfaces of samples under mode I. In the reference samples (Fig. 8-A & B), fiber breakage, fiber/matrix debonding, and matrix cracking, occurring during delamination and crack propagation, are evident. Matrix cracking in this loading mode appears brittle and cleaved. Generally, the fracture surfaces appear smooth, indicating limited resistance to interlaminar crack propagation and suggesting low fracture toughness. Furthermore, the fracture surface images of the modified samples (Fig. 8-C & D) reveal the presence of polysulfone nanoparticles dispersed throughout the matrix, forming a secondary phase with the brittle epoxy. Upon careful examination of these images, it is evident that the fracture surface exhibits a rougher texture compared to the reference samples. Additionally, island-shaped regions have been created on the fracture surface shown by orange ellipsoids (Fig. 8-C). The presence of these island-shaped areas indicates that the crack direction continuously changes between the upper and lower layers, rather than following a straight path. This can enhance the fracture toughness and also modified the delamination behavior. Moreover, under a magnification of 1000X, Fig. 8-D illustrates spherical polysulfone nanoparticles, half of which are embedded within the matrix (core patterns), indicated by red arrows. The presence of hollow cavities also signifies the imprint left by nanoparticles on the opposing fracture surface. This pattern of core and cavity indicates that during mode I loading, the crack, upon encountering a brittle region, diverts its path upon reaching a softer region, thereby bypassing the spherical thermoplastic particles before continuing its propagation. Finally presence of the PSU particles at the crack interfaces, improves the mechanical interlocking between layers.

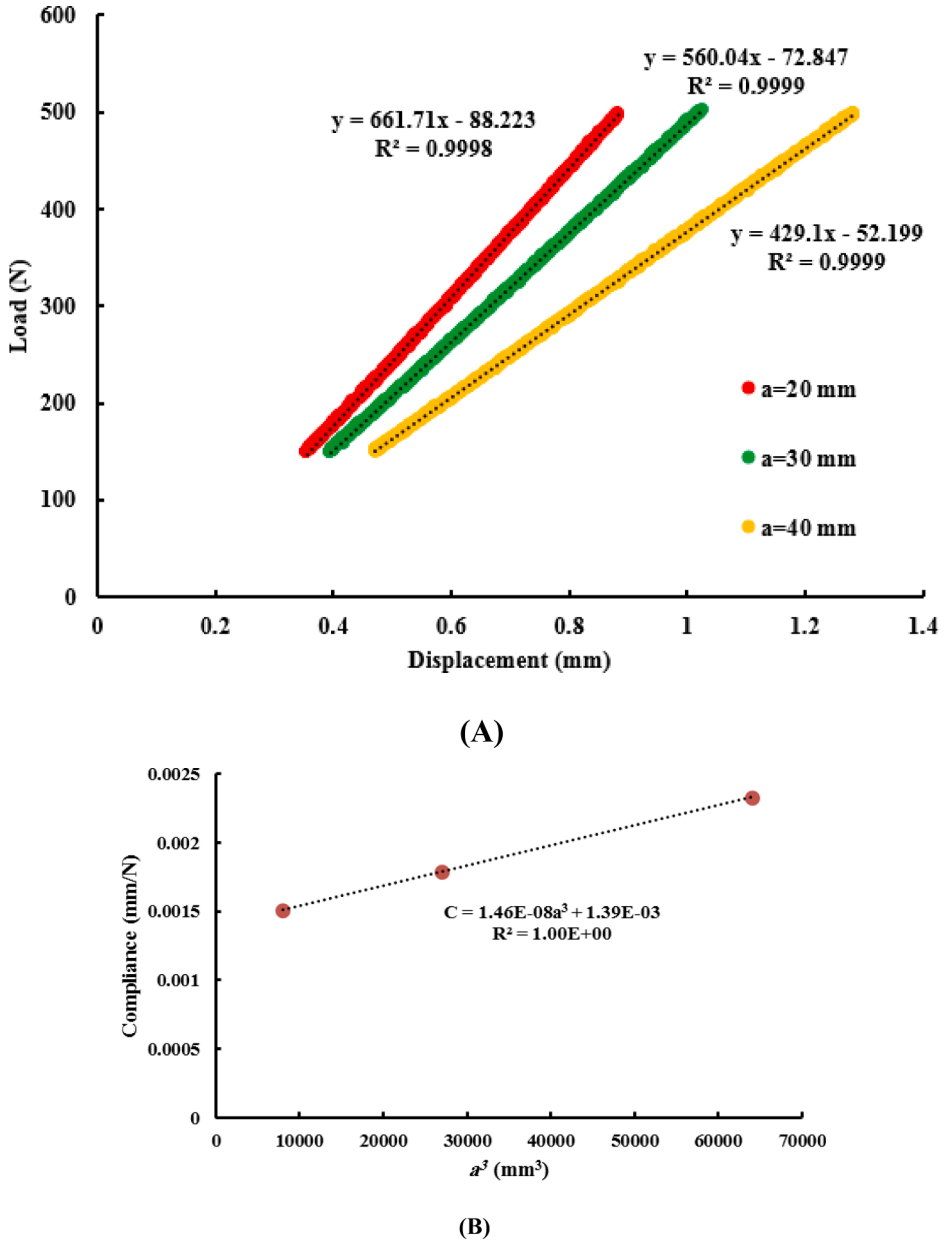

Fig. 7. Determining compliance coefficients for PSU-4 modified specimen A) load - displacement graphs for three different length of initial cracks and calculation of specimen stiffness at each crack length B) Compliance vs third power of initial crack length.

Table 3
Mode II test results and related parameters.

Sample	P_{cr} (N)	Ave. P_{cr} (N)	δ_{max} (mm)	B (mm)	a_0 (mm)	A (mm/N)	m (1/N.mm^2)	G_{IIC} (J/m^2)	Ave. G_{IIC} (J/m^2)
Ref-4	1110	1096.6 ± 50.7	2.02	25	30	1.39E-03	1.41E-08	938	954.6 ± 50.4
Ref-5	1029	CV=0.04	1.98	25	30	1.42E-03	1.58E-08	903	CV=0.05
Ref-6	1151		2.16	25	30	1.45E-03	1.43E-08	1023	
PSU-4	1086	1099.6 ± 25.2	2.07	25	30	1.39E-03	1.46E-08	930	949.6 ± 13.9
PSU-5	1135	CV=0.02	2.11	25	30	1.37E-03	1.38E-08	959	CV=0.01
PSU-6	1078		2.04	25	30	1.36E-03	1.53E-08	960	

Fig. 9 displays fractured surfaces of samples subjected to mode II loading. As depicted in this figure, compared to mode I, the fracture surfaces of reference samples appear rougher. Notably, instead of observing fiber fracture, the fiber imprints are prevalent (Fig. 9-A), suggesting the occurrence of fiber/matrix debonding. An important observation is the non-cleavage of matrix fracture in mode II condition, unlike mode I. Matrix cracking in this mode is characterized by the form of cusp features (Fig. 9-B). Microscopically, cusps arise from the development of angled matrix cracks within the delamination region. Some researchers [51,52] attribute the enhancement in mode II fracture toughness to the development of these cusp features. The formation of cusps can absorb more energy, consequently increasing fracture

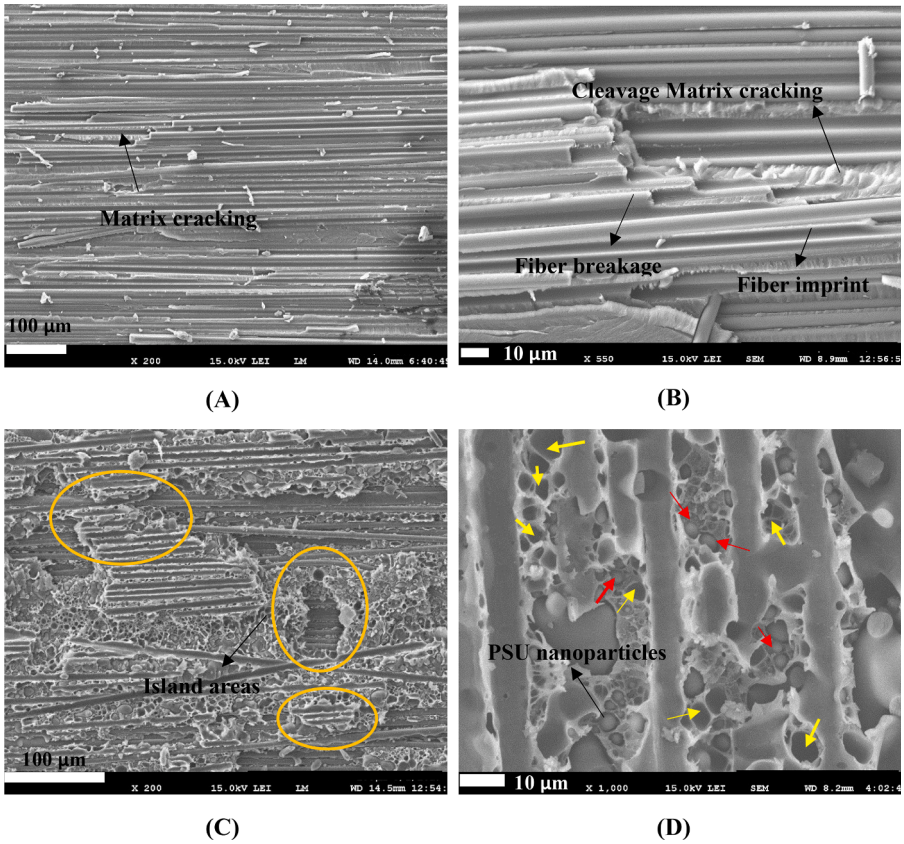

Fig. 8. The Mode I damage features of **A**,B) reference samples and **C**,D) TNPs-modified samples.

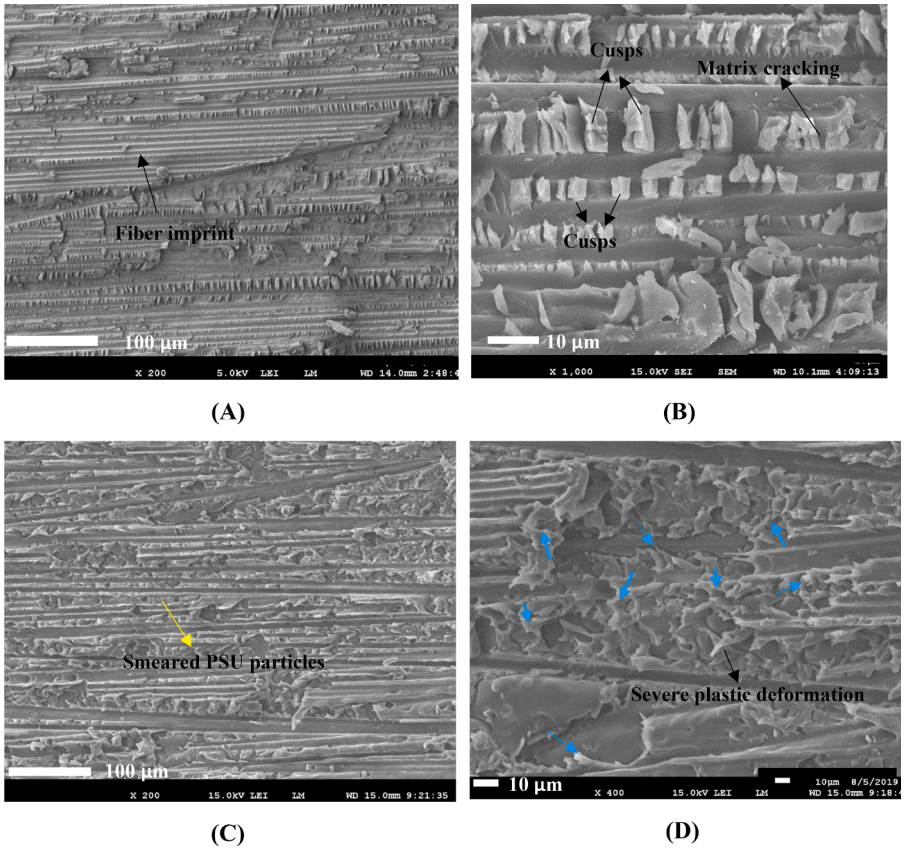

Fig. 9. The SEM micrograghes of fractured surface in Mode II test **A**,B) reference **C**,D) TNPs-modified.

toughness.

In Figs. 9-C&D, fractured surface of TNPs-modified sample under mode II loading is depicted. Surprisingly, no cusps are observed in this case; instead, thermoplastic polysulfone nanoparticles are observed to be smeared across the fracture surface (Fig. 9-D). Furthermore, unlike in mode I, the presence of core and cavity patterns is not evident in this instance. Additionally, in some regions, the polysulfone particles exhibit severe plastic deformation, as indicated by blue arrows in Fig. 9-D. Despite the absence of cusps in this scenario, the severe plastic deformation of the soft nanoparticles causes energy absorption, thereby preventing a reduction in fracture toughness. It appears that the energy that would typically contribute to cusp formation in this loading scenario is instead utilized for the plastic deformation of nanoparticles. Consequently, the fracture toughness of mode II remains unchanged in both reference and modified specimens.

Fig. 10 schematically shows the toughenning mechanism by thermoplastic polysulfone nanoparticles in both mode I and mode II. As seen in Fig. 10-A, in mode I, the interlaminar crack navigates around the nanoparticles, changing directions successively, thereby enhancing the mode I fracture toughness. Under mode II conditions (Fig. 10-B), due to shear stress, the main crack directly passes through the thermoplastic nanoparticles, causing them to break into two pieces. Because the nanoparticles have limited resistance to shear stress, their effect on fracture toughness is minimal.

7. Conclusion

This work aims to assess the influence of thermoplastic nanoparticles of polysulfone (TNPs) on the delamination resistance of carbon epoxy laminates and to comparatively analyze this influence in mode I and mode II tests. Initially, polysulfone pellets were transformed into nanofibers mat using the electrospinning method. These nanofibers were then positioned between the CFRP laminates. With an increase in temperature, the viscosity of resin decreased, enabling it to flow into the microcavities of the nanofibers. Subsequently, by raising the temperature to 180° for the final curing of the epoxy resin, the polysulfone melted and dispersed uniformly within the brittle epoxy as a matrix. After preparation of specimens, both mode I and mode II loading were applied to examine the behavior of thermoplastic polysulfone nanoparticles under these two distinct loading conditions. Results indicated a 1.9-fold enhance in mode I fracture toughness, while no significant change in mode II fracture toughness was observed. To understand the reasons behind this phenomenon, SEM analysis was employed. Microscopic images revealed that during mode I test, the crack line continuously altered its direction due to contact with polysulfone nanoparticles, thereby increasing the fracture toughness. Conversely, in mode II test, the crack propagated directly through the polysulfone nanoparticles, resulting in minimal alteration to the fracture toughness.

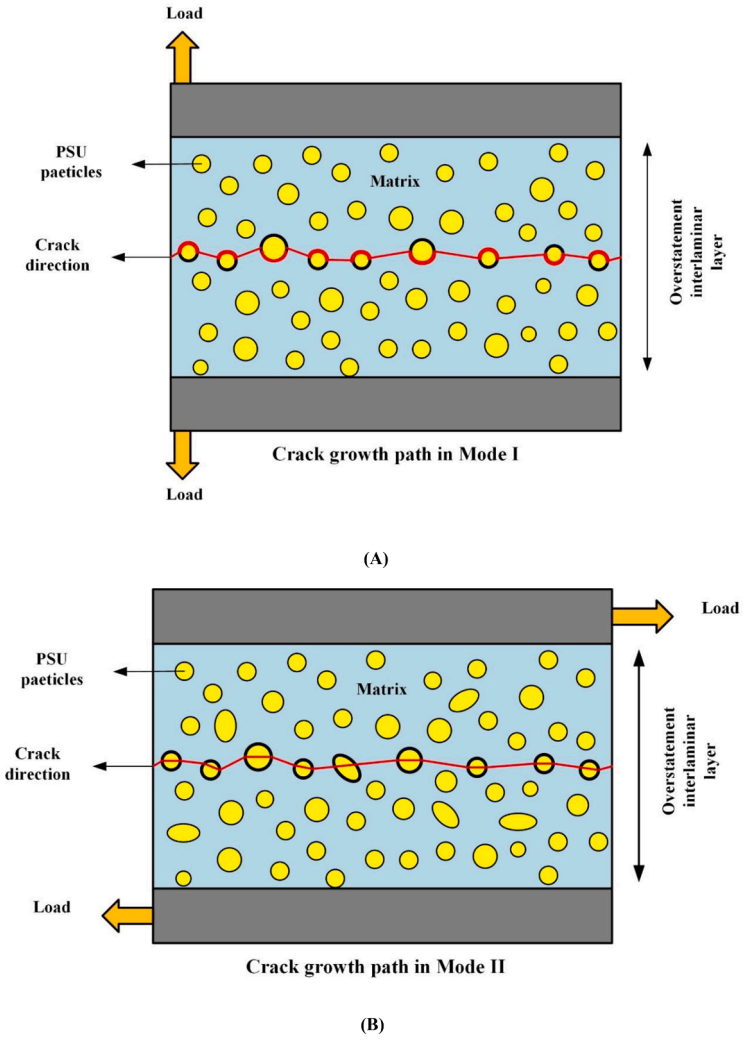

Fig. 10. The schematic of interlaminar crack propagation of thermoplastic nanoparticles modified laminates in A) Mode I and B) Mode II.

CRediT authorship contribution statement

Reza Mohammadi: Writing – original draft, Methodology, Conceptualization. **R Akrami:** Writing – review & editing, Writing – original draft, Conceptualization. **Maher Assaad:** Validation, Methodology, Funding acquisition, Conceptualization. **Ahmed Imran:** Validation, Investigation, Funding acquisition, Data curation. **Mohammad Fotouhi:** Writing – review & editing, Supervision, Funding acquisition, Conceptualization.

Declaration of competing interest

The authors declare that they have no known competing financial interests or personal relationships that could have appeared to influence the work reported in this paper.

Data availability

The authors do not have permission to share data.

Acknowledgements

This research work has been supported from and the UK Engineering and Physical Sciences Research Council (EP/V009451/1) and Ajman University (2023-IRG-ENIT-32). All essential documents are provided within the paper.

References

[1] H. Liu, G. Qi, G. Renaud, G. Li, C. Li, Application of the effective crack length method to model delamination of unidirectional composite laminates under Mode II shear loadings, Composites Part C: Open Access 12 (2023) 100401.
[2] R. Mohammadi, M. Saeedifar, H.H. Toudeshky, M.A. Najafabadi, M. Fotouhi, Prediction of delamination growth in carbon/epoxy composites using a novel acoustic emission-based approach, J. Reinf. Plast. Compos. 34 (2015) 868–878.
[3] Y. Fu, X. Yao, A review on manufacturing defects and their detection of fiber reinforced resin matrix composites, Composites Part C: Open Access 8 (2022) 100276.
[4] A. Vescovini, J.A. Cruz, D. Ma, C. Colombo, A. Salerno, O. Bianchi, et al., Experimental investigation on low-velocity impact behavior of glass, Kevlar, and hybrid composites with an elastomeric polyurethane matrix, Composites Part C: Open Access 13 (2024) 100426.
[5] Z. Yu, S Gao, Increase of contact radius due to deflection in low velocity impact of composite laminates and prediction of delamination threshold load, Compos. Struct. 147 (2016) 286–293.
[6] A. Tabatabaeian, R. Mohammadi, P. Harrison, M. Fotouhi, Characterisation and Application of Bio-Inspired Hybrid Composite Sensors for Detecting Barely Visible Damage under Out-of-Plane Loadings, Sensors, 24 (16) (2024) 5170, https://doi.org/10.3390/s24165170. Article.
[7] M.L.J. Suman, S.M. Murigendrappa, S. Kattimani, Characterisation of fatigue delamination growth in plain woven hybrid laminated composites subjected to Mode-I loading, Theoretical and Applied Fracture Mechanics 129 (2024) 104236.
[8] L. Yao, M. Chuai, J. Liu, L. Guo, X. Chen, R.C. Alderliesten, et al., Fatigue delamination behavior in composite laminates at different stress ratios and temperatures, Int. J. Fatigue 175 (2023) 107830.
[9] A. Quinlan, O. Castro, J.M. Dulieu-Barton, Towards assessment of fatigue damage in composite laminates using thermoelastic stress analysis, Composites Part C: Open Access 12 (2023) 100377.
[10] L. Maragoni, P.A. Carraro, M. Simonetto, M. Quaresimin, A novel method to include crack-induced delamination in a fatigue damage predictive procedure for composite laminates, Compos. Sci. Technol. 238 (2023) 110011.
[11] L. Yao, M. Chuai, H. Li, X. Chen, D. Quan, R.C. Alderliesten, et al., Temperature effects on fatigue delamination behavior in thermoset composite laminates, Eng. Fract. Mech. 295 (2024) 109799.
[12] J. Pernas-Sánchez, S.M. García-Rodríguez, J.A. Artero-Guerrero, J. López-Puente, J. Costa, High velocity impact response of carbon/epoxy composite laminates at cryogenic temperatures, Compos. Part A Appl. Sci. Manuf. 168 (2023) 107456.
[13] J. Cao, J. Gu, Z. Dang, C. Zhang, On temperature-dependent fiber bridging in mode I delamination of unidirectional composite laminates, Compos. Part A Appl. Sci. Manuf. 171 (2023) 107581.
[14] A. Delbariani-Nejad, A. Farrokhabadi, M. Fotouhi, Finite element reliability analysis of edge delamination onset due to interlaminar stresses in composite laminates, Compos. Struct. 288 (2022) 115410.
[15] L. Shen, L. Liu, Y. Zhou, Z. Wu, Thickness effect of carbon nanotube interleaves on free-edge delamination and ultimate strength within a symmetric composite laminate, Compos. Part A Appl. Sci. Manuf. 132 (2020) 105828.
[16] M. Hajikazemi, W. Van Paepegem, A variational model for free-edge interlaminar stress analysis in general symmetric and thin-ply composite laminates, Compos. Struct. 184 (2018) 443–451.
[17] R. Mohammadi, M. Assaad, A. Imran, M. Fotouhi, Fractographic analysis of damage mechanisms dominated by delamination in composite laminates: a comprehensive review, Polym. Test. 134 (2024) 108441.
[18] V. Moorthy, K. Marappan, Experimental study on delamination identification in tapered laminated composite plates using damage detection models, Compos. Struct. 323 (2023) 117494.
[19] T. Gordon, M.R. Wisnom, B.C. Kim, Suppression of compression induced delamination in tapered laminated composites using a ply scarfing method, Compos. Part A Appl. Sci. Manuf. 176 (2024) 107870.
[20] S.H. Dashatan, L. Parnas, D. Coker, M.O. Bozkurt, E.B. Ozen, In-situ observation and numerical study of dynamic delamination in tapered composite laminates, Compos. Struct. 312 (2023) 116841.
[21] S.O. Ismail, S.O. Ojo, H.N. Dhakal, Thermo-mechanical modelling of FRP cross-ply composite laminates drilling: delamination damage analysis, Composites Part B: Engineering 108 (2017) 45–52.
[22] R. Higuchi, S. Warabi, W. Ishibashi, T. Okabe, Experimental and numerical investigations on push-out delamination in drilling of composite laminates, Compos. Sci. Technol. 198 (2020) 108238.
[23] Kumar G Rampal, S.M. Rangappa, S. Siengchin, S Zafar, A review of recent advancements in drilling of fiber-reinforced polymer composites, Composites Part C: Open Access 9 (2022) 100312.
[24] R. Mohammadi, M. Saeedifar, M. Ahmadi Najafabadi, H. Hosseini Toudeshky, Acoustic Emission Based Methodology to Evaluate the Fracture Toughness in Carbon/Epoxy Composites, Amirkabir J. Mech. Eng. 49 (2) (2017) 379–386.
[25] R. Mohammadi, M.A. Najafabadi, H. Saghafi, D. Zarouchas, Fracture and fatigue behavior of carbon/epoxy laminates modified by nanofibers, Compos. Part A Appl. Sci. Manuf. 137 (2020) 106015.
[26] J. Cao, B. Jiang, Z. Li, Z. Dang, C. Zhang, Evaluating the loading rate dependency of mode I delamination for composite laminates at different temperatures, Compos. Sci. Technol. 249 (2024) 110505.
[27] R. Mohammadi, M.A. Najafabadi, H. Saghafi, M. Saeedifar, D. Zarouchas, The effect of mode II fatigue crack growth rate on the fractographic features of CFRP composite laminates: an acoustic emission and scanning electron microscopy analysis, Eng. Fract. Mech. 241 (2021) 107408.
[28] K.O. Low, M. Johar, A.N. Sung, M.N. Mohd Nasir, S.S. Rahimian Koloor, M. Petrů, et al., Displacement rate effects on mixed-mode I/II delamination of laminated carbon/epoxy composites, Polym. Test. 108 (2022) 107512.
[29] S.I.B. Syed Abdullah, S.K. Bokti, K.J. Wong, M. Johar, W.W.F. Chong, Y. Dong, Mode II and mode III delamination of carbon fiber/epoxy composite laminates subjected to a four-point bending mechanism, Composites Part B: Engineering 270 (2024) 111110.
[30] ASTM D7522, Standard Test Method For Pull-Off Strength For FRP Laminate Systems Bonded to Concrete Substrate, ASTM International, West Conshohocken, PA, 2021.
[31] A. Knopp, E. Funck, A. Holtz, G. Scharr, Delamination and compression-after-impact properties of z-pinned composite laminates reinforced with circumferentially notched z-pins, Compos. Struct. 285 (2022) 115188.
[32] S. Fei, W. Wang, H. Ding, H. Wang, J. Li, Y. Ke, Strengthening of composite T-joints using Ø 0.11 mm Z-pins via an ultrasound-guided insertion process, Composites Part C: Open Access 8 (2022) 100268.
[33] M.N. Saleh, H.M. El-Dessouky, M. Saeedifar, S.T. De Freitas, R.J. Scaife, D. Zarouchas, Compression after multiple low velocity impacts of NCF, 2D and 3D woven composites, Compos. Part A Appl. Sci. Manuf. 125 (2019) 105576.
[34] M. Saeedifar, M.N. Saleh, H.M. El-Dessouky, S. Teixeira De Freitas, D Zarouchas, Damage assessment of NCF, 2D and 3D woven composites under compression after multiple-impact using acoustic emission, Compos. Part A Appl. Sci. Manuf. 132 (2020) 105833.
[35] D. Shu, Y.-W. Mai, Effect of stitching on interlaminar delamination extension in composite laminates, Compos. Sci. Technol. 49 (1993) 165–171.
[36] M. Ravandi, W.S. Teo, L.Q.N. Tran, M.S. Yong, T.E. Tay, The effects of through-the-thickness stitching on the Mode I interlaminar fracture toughness of flax/epoxy composite laminates, Mater. Des. 109 (2016) 659–669.
[37] L. Francesconi, F. Aymerich, Numerical simulation of the effect of stitching on the delamination resistance of laminated composites subjected to low-velocity impact, Compos. Struct. 159 (2017) 110–120.
[38] A. Gholizadeh, M.A. Najafabadi, H. Saghafi, R. Mohammadi, Considering damages to open-holed composite laminates modified by nanofibers under the three-point bending test, Polym. Test. 70 (2018) 363–377.
[39] H. Saghafi, A. Nikbakht, R. Mohammadi, D. Zarouchas, The Thickness Effect of PSF Nanofibrous Mat on Fracture Toughness of Carbon/Epoxy Laminates, Materials. (Basel) (2021).
[40] M. Saeedifar, H. Saghafi, R. Mohammadi, D. Zarouchas, Temperature dependency of the toughening capability of electrospun PA66 nanofibers for carbon/epoxy laminates, Compos. Sci. Technol. 216 (2021) 109061.
[41] R. Mohammadi, M.A. Najafabadi, H. Saghafi, D. Zarouchas, Mode-II fatigue response of AS4/8552 carbon /epoxy composite laminates interleaved by electrospun nanofibers, Thin-Walled Struct. 154 (2020) 106811.
[42] R. Rafiee, M. Sahraei, Characterizing delamination toughness of laminated composites containing carbon nanotubes: experimental study and stochastic multi-scale modeling, Compos. Sci. Technol. 201 (2021) 108487.
[43] J. Song, Y. Zhang, H. Fan, T. Hu, L. Hu, J. Qu, Design of interfaces for optimal mechanical properties in Al2O3/Mo laminated composites, J. Eur. Ceram. Soc. 35 (2015) 1123–1127.

[44] V. Prasad, K. Sekar, S. Varghese, M.A. Joseph, Evaluation of interlaminar fracture toughness and dynamic mechanical properties of nano TiO2 coated flax fibre epoxy composites, Polym. Test. 91 (2020) 106784.
[45] Y. Liu, A. Zou, Wang G-d, C. Han, E Blackie, Enhancing interlaminar fracture toughness of CFRP laminates with hybrid carbon nanotube/graphene oxide fillers, Diam. Relat. Mater. 128 (2022) 109285.
[46] V. Prasad, K. Sekar, S. Varghese, M.A. Joseph, Enhancing Mode I and Mode II interlaminar fracture toughness of flax fibre reinforced epoxy composites with nano TiO2, Compos. Part A Appl. Sci. Manuf. 124 (2019) 105505.
[47] HexPly ® 8552 Epoxy matrix (180 °C/356°F Curing matrix) in FTA 072e, Hexcel Composites Publication, 2013.
[48] R. Mohammadi, R. Akrami, M. Assaad, M. Nasor, A. Imran, M. Fotouhi, Polysulfone nanofiber-modified composite laminates: investigation of mode-I fatigue behavior and damage mechanisms, Theor. Appl. Fracture Mech. 127 (2023) 104078.
[49] ASTM D 5528-13, Standard Test Method For Mode I Interlaminar Fracture Toughness of Unidirectional Fiber-Reinforced Polymer Matrix Composites, ASTM International, West Conshohocken, PA, 2022, 2022.
[50] ASTM D7905, Standard Test Method For Determination of the Mode II Interlaminar Fracture Toughness of Unidirectional Fiber-Reinforced Polymer Matrix Composites, ASTM International, West Conshohocken, PA, 2019, 2019.
[51] E.S. Greenhalgh, C. Rogers, P. Robinson, Fractographic observations on delamination growth and the subsequent migration through the laminate, Compos. Sci. Technol. 69 (2009) 2345–2351.
[52] Rogers C., Greenhalgh E., Robinson P. Developing a mode ii fracture model for composite laminates. 2008.